Supporting Information for

A Manganese Alternative to Gadolinium for MRI Contrast

Eric M. Gale,* Iliyana P. Atanasova, Francesco Blasi, Ilknur Ay, and Peter Caravan*

The Athinoula A. Martinos Center for Biomedical Imaging, Department of Radiology, Massachusetts General Hospital, Harvard Medical School, 149 Thirteenth Street, Suite 2301, Charlestown, Massachusetts 02129.

Experimental Methods.

General. All chemicals and solvents were purchased commercially and used without further purification.

NMR. NMR spectra were recorded on a 500 MHz Varian spectrometer at 25 °C unless otherwise noted. Chemical shifts are reported in δ (ppm). For ^{1}H and ^{13}C NMR spectra, the residual solvent peaks were used as internal reference except for ^{13}C and ^{19}F NMR recorded in D_2O where dioxane and potassium fluoride were used as the internal references, respectively.[1] Relaxivity measurements were performed on a Bruker mq60 Minispec, 1.41 T and 37 °C. Longitudinal (T_1) relaxation was acquired via an inversion recovery experiment using 10 inversion times of duration ranging between 0.05 × T_1 and 5 × T_1; tranverse (T_2) relaxation was measured using a Carl-Purcell-Meiboom-Gill spin-echo experiment. Relaxivity ($r_{1,2}$) was determined from the slope of a plot of $1/T_{1,2}$ vs. [Mn] for at least 4 concentrations. The transverse (T_2) relaxation times of ^{17}O were acquired at 11.7 T from the full-width at half-height of the $H_2{}^{17}O$ signal.[2] ^{17}O T_2 relaxivity (r_2^O) was calculated by dividing the Mn-imparted increase in $1/T_2$ relative to neat H_2O (pH 3) by the Mn concentration in mM. 0.7-1.0 mL NMR samples were enriched with a 10 μL of 18% $H_2{}^{17}O$.

Relaxivity in the presence of fibrin clots. The measurements were performed as previously described.[3] Briefly, $CaCl_2$ was added to a solution of Mn-FBP, thrombin and human fibrinogen to trigger fibrin formation (final concentrations of $CaCl_2$, fibrinogen and thrombin were 10 mM, 10 mg/mL and 0.6 U/mL, respectively). The resultant fibrin gels were incubated for 20 min at 37 ºC before measurement.

HPLC methods. Liquid chromatography-mass spectrometry (LC-MS) was performed using an Agilent 1100 Series apparatus with an LC/MSD trap and Daly conversion dynode detector with UV detection at 220, 254, and 280 nm. The methods used on this system are as follows: (A1) Luna C18 column (100 × 2 mm); eluent A: H_2O/0.1 % formic acid, B: MeCN/0.1 % formic acid; gradient: 5 % B to 95 % B over 9 min; flow rate 0.8 mL/min (used for characterization of organic compounds), (A2) Kromasil C18 column (250 × 4.6 mm); eluent C: 95 % MeCN/5 % 10 mM ammonium acetate, D: 10 mM ammonium acetate; gradient 5 % C to 95 % C over 14 min; flow rate 0.8 mL/min (used for characterization of chelates and manganese complexes), (A3) Luna C18 column (100 × 2 mm); eluent A: H_2O/0.1 % formic acid, B: MeCN/0.1 % formic acid; gradient: 5 % B to 95 % B over 3 min, than 95% B over 3 min; flow rate 0.8 mL/min (used for characterization of organic compounds). Reverse-phase semi-preparative purification was performed on the Rainin Dynamax HPLC system with UV detection from 220 to 280 nm using a Phenomenex C18 or C5 column (250 x 21.8 cm). The mobile phase A was water with 0.1% TFA added; mobile phase B was MeCN with 0.1% TFA added; mobile phase C was 50 mM ammonium acetate buffer, pH 6.5; mobile phase D was a mixture of 5 % 50 mM ammonium acetate buffer, pH 6.5 and 95% MeCN. The methods used for purification are as follows: (P1) starting from 80% A/ 20% B,

the fraction of B increased to 95 % over 23 min. The column was washed with 95 % B for 2 min and then ramped to 5 % B. The system was re-equilibrated at 5% B for 3 min, (P2) starting from 95% C/ 5% D, the fraction of D increased to 60 % over 23 min. The column was washed with 95 % B for 2 min and then ramped to 5 % B. The system was re-equilibrated at 5% B for 3 min, (P3) starting from 95% A/ 5% B, the fraction of B increased to 60 % over 40 min. The column was washed with 95 % B for 2 min and then ramped to 5 % B. The system was re-equilibrated at 5% B for 3 min.

Potentiometric titration. pH-potentiometric measurements were performed using an MPT 798 Titrino equipped with an Orion ROSS Ultra pH electrode and temperature-controlled reaction vessel held at 298K. A standardized solution of 0.15 M NaOH was used as the titrant. Samples were purged with Ar prior to measurement, and an inert atmosphere was maintained by constant Ar passage over the titration vessel. The electrode was calibrated prior to each titration by titrating a standardized $HCl_{(aq)}$ solution at ionic strength 0.15 using NaCl as the inert electrolyte with the standardized NaOH titrant. A working slope and intercept were generated by plotting mV as a function of calculated pH, which enabled direct conversion of electrode readings to $[H^+]$ during sample titrations. pH values recorded during the titrations refers to hydrogen ion concentration. All titration samples were prepared in solutions of 0.15M NaCl in distilled, de-ionized water. Ligand solutions were prepared by dissolving a weighed quantity into the electrolyte and concentration was calculated from the effective weight of the ligand. Titration of PyC3A•TFA revealed 4 ionization events and ligand concentration was confirmed from the moles of NaOH consumed between the inflection points in the titration curve. Solutions of 1:1 ligand: Mn were prepared by adding an appropriate volume of standardized $MnCl_2$ in 0.15M NaCl electrolyte to a weighted quantity of ligand. All titrations were performed in triplicate. The data was analyzed using the Hyperquad2013 software package.[4]

DD(E) binding assay. The affinity of the probes was assessed using a DD(E) fluorescence polarization displacement assay that was described previously.[5] The displacement of a tetramethylrhodamine labeled peptide (TRITC-Tn6) from DD(E) was detected by observing the corresponding change in fluorescence anisotropy. The K_d of the TRITC-Tn6 probe was determined by titrating it with the DD(E) protein and fitting the resultant fluorescence data as described previously.[5] This experiment was performed at room temperature using a concentration of TRITC-Tn6 of 0.1 μM in the following assay buffer: Tris base (50 mM), NaCl (100 mM), CaC_{l2} (2 mM), Triton X- 100 (0.01%), pH = 7.8. The anisotropy measurements were made using a TECAN Infinity F200 Pro plate reader equipped with the appropriate filter set for tetramethylrhodamine (excitation 535 nm, emission 590 nm).

Mn quantification in tissues and blood. Metal concentrations were determined using an Agilent 8800-QQQ

ICP-MS system. All samples were diluted with 0.1 % Triton X-100 in 5 % nitric acid. A linear calibration curve for each metal ranging from 0.1 ppb to 200 ppb was generated daily for the quantification. LC-ICP-MS data were acquired by diverting the LC mobile phase (method A2) into the ICP-MS functioning in time resolved analysis mode. Lutetium internal standard was steadily introduced to the ICP-MS from an external source during the analysis. Linear calibration curves were generated daily by from the area under the LC peak corresponding to independently isolated Mn species run at multiple concentrations (calibration curves generated from plotting either Mn or Mn/Lu cps against known concentration yielded identical identical data).

Estimates of albumin binding. Measurements were performed on a series of solutions ranging between 150-300 μM $[Mn(PyC3A)(H_2O)]^-$ in either 4.5% wt/v BSA or bovine blood plasma. 150 μL of each solution was placed within a Millipore Ultra Free MC 5 kDa cutoff filtration vessel and ~10 μL of the solution was forced through the filter by centrifugation. Mn content in each unfiltered solution and filtrate were quantified by ICP-MS. The percentage of $[Mn(PyC3A)(H_2O)]^-$ bound to albumin was estimated from the difference in Mn concentrations between unfiltered solution and filtrate.

Rat model of carotid artery thrombosis. All experiments were performed in accordance with the National Institutes of Health Guide for the Care and Use of Laboratory Animals[6] and were approved by the Institutional Animal Care and Use Committee at Massachusetts General Hospital. Adult male Wistar rats (N =4; weight, 200–300 g; Charles River Laboratories) were used for this study. Arterial thrombosis was induced by application of 25% w/v $AlCl_{3(aq)}$ to the vessel outer wall. Under isoflurane anesthesia, the right common carotid artery was exposed, and a small strip of filter paper soaked in the $AlCl_3$ solution was applied. Injury was performed 1–2 cm proximal to carotid bifurcation by the same investigator to minimize variability. The femoral artery was catheterized using PE-50 tubing (Fisher Scientific) for probe injection. Probes were injected 30 min after thrombus formation. Each rat was injected with 0.01 mmol/kg probe (0.04 mmol/kg based on metal ion). For blood draw experiments, rats were catheterized in the femoral vein and artery for injection and sampling, respectively. Blood was drawn at 2, 5, 10, 15, 30, 60 and 120 min, than 24h after injection and collected in heparinized vials. Immediately after collection a portion of the blood was centrifuged for 10 min at 5000 rpm and the plasma separated and weighed, diluted 2x with PBS buffer and injected onto the analytical HPLC column.

MR imaging of mice. Healthy balb/C male mice (N=4, Charles River Laboratories, Cambridge, MA) were imaged at 4.7T using a small bore animal scanner (Bruker Biospec) with a custom-built volume coil. The imaging protocol at baseline consisted of multislice two-dimensional rapid acquisition with refocused echo (RARE) imaging to delineate anatomy and a 3D fast low-angle shot (FLASH) sequence. After tail-veil vein

administration of 60 μmol/kg of Na[Mn(PyC3A)(H_2O)], the FLASH sequence used at baseline was repeated for 90 minutes following contrast delivery. FLASH imaging parameters: coronal orientation, TR/TE/flip angle=15.3 ms/1.54 ms/40°, in-plane FOV = 48x28 mm, matrix=192×112, 96 slices, slice thickness = 0.25 mm, voxel size = 0.25 x 0.25 x 0.25 mm, 1 average, and acquisition time = 2:53 minutes. Images were analyzed in Matlab by drawing regions of interest (ROI) and measuring signal intensity (SI) of the kidneys, liver, left ventricle, and muscle. The standard deviation (SD) of an ROI taken in the air outside the animal was used to estimate noise. Signal to noise ration (SNR) for each tissue type was calculated as (SI_{tissue})/(SD_{air}). Normalized SNR (nSNR) was calculated by dividing SNR at each time point post probe injection by the SNR prior to injection. Contrast agent washout was analyzed by plotting nSNR vs time curves and fitting the decay to a monoexponential function.

MR imaging of thrombosis in rats. Imaging was performed on a human whole-body 1.5T system (Avanto, Siemens Healthcare, Erlangen, Germany) with a custom-built transmit-receive coil. Animals were anesthetized with isoflurane (1–2%) for the duration of the experiment. Catheters were placed in the femoral vein and the femoral artery for blood draws and contrast administration, respectively. First, the head and neck were visualized with T_1-weighted images in sagittal, coronal, and axial planes, followed by a 3D TOF angiogram acquired transversely. Next molecular imaging was performed at baseline with two different sequences: 3D T_1-weighted gradient echo (GRE) and 2D T_1-weighted dark-blood fast spin echo (DB-TSE). After all pre-contrast scans were completed, 0.01 mmol/kg of the imaging probe, either EP-2104R or Mn-FBP, was injected as a bolus via the femoral artery. The molecular imaging sequences used at baseline were repeated for 60 minutes following contrast delivery. The TOF angiogram was acquired with the following parameters: 3D T_1-weighted gradient echo sequence, TR/TE/flip angle=26 ms/5.75 ms/25°, in-plane FOV = 85x85 mm, matrix=320×320, 58 slices, slice thickness = 0.47 mm, voxel size = 0.3 x 0.3 x 0.47 mm, 1 average, and acquisition time = 4:18 minutes. The GRE sequence for molecular imaging had identical parameters to the TOF angiogram, but smaller head-to-foot coverage (48 slices) and longer TR (35 ms) resulting in a scan time of 6:34 minutes. In addition, inferior saturation was performed to null inflowing arterial blood. DB-TSE was performed with TR/TE = 800 ms/20 ms, in-plane FOV = 85x85 mm, matrix=320×320, 11 slices, slice thickness = 2 mm, voxel size = 0.3 x 0.3 x 2 mm, echo train length = 11, 1 average, and acquisition time = 4 minutes. GRE and DB-TSE had overlapping volumetric coverage and were acquired with axial orientation. Images were analyzed in Matlab (Version R2104a, MathWorks, Natick, MA) by drawing ROIs and measuring mean SI of the clot, contralateral artery, and adjacent muscle. Noise was quantified as the standard deviation (SD) of the signal measured in the air outside the animal. SNR was calculated as described above for each tissue type. We also calculated contrast-

to-noise ratios for the clot and the contralateral artery relative to muscle: $CNR = (SI_{tissue} - SI_{adj\ muscle})/SD_{air}$. SNR and CNR were estimated at baseline (SNR_{pre} and CNR_{pre}) from pre-contrast images and at various time points after contrast injection (SNR_{post} and CNR_{post}). Normalized SNR (nSNR) values were obtained by dividing SNR at each time point by SNR_{pre}. Unpaired Student's t-Test was used for statistical analysis where $p < 0.05$ was considered as significant.

Histology. Carotid arteries were harvested 90 min after generation of induction of thrombosis, carefully rinsed in phosphate buffer, embedded in OCT mounting media (Tissue-Tek) and snap-frozen in -45 ºC isopentane. Arteries were cryosectioned in 20 μM slices and processed for Hemotoxylin and Eosin staining according to the standard protocol. Images were acquired using a Nikon TE-2000 microscope (40x magnification).

Synthesis. Compound **5** was prepared as previously described.[7] Synthesis of all other compounds are described below.

***N*-benzyl-*trans*-1,2-diaminocyclohexane (1)**. To a batch of 7.113 g (62.29 mmol) 1,2-diaminocyclohexane in 50 mL MeCN was added dropwise 1.093 g (6.39 mmol) benzyl bromide in 10 mL MeCN at room temperature over the course of 1 hour. After 16 hours, the resultant white, heterogeneous solution was concentrated to dryness and partitioned between CH_2CI_2 and satd. $Na_2CO_{3(aq)}$. The layers were separated and the organic phase washed again with satd. $Na_2CO_{3(aq)}$ then brine, dried over Na_2SO_4 and concentrated to 1.280 g (6.26 mmol, 98%) of **1** as a light yellow oil. ^{1}H NMR (500 MHZ, $CDCl_3$, δ from TMS): 7.36-7.22 (m, 5H), 3.94 (d, 1H), 3.69 (d, 1H), 2.38 (m, 1H), 2.09 (m, 2H), 1.90 (m, 1H), 1.73 (m, 2H), 1.32-1.09 (m, 4H). ESI-MS: *m/z* = 205.3 $[M+H]^+$; calcd.: 205.3.

***N*-benzyl-*N,N',N'-trans*-l,2-cyclohexylenediaminetri-*tert*-butylacetate (2)**: To 1.133 g (5.55 mmol) **1**, 4.194 g (32.35 mmol) diisopropylethylamine and 0.966 g (5.82 mmol) potassium iodide in 5 mL DMF was added 5.340 g (27.38 mmol) ^{t}butyl bromoacetate at room temperature. The resultant tan, heterogeneous solution was stirred for 6 hours before dilution with Et_2O followed by washing with satd. $K_2CO_{3(aq)}$, several changes of water and brine, drying over Na_2SO_4 and concentration to 5.468 g brown oil. Flash chromatography (silica gel, 19:1 to 4:1 hexane:EtOAc) yielded pure **2** as 1.949 g (3.57 mmol, 64%) of light yellow oil. ^{1}H NMR (500 MHZ, $CDCl_3$, δ from TMS): 7.45 (d, 1H), 7.30 (t, 1H), 7.23 (d, 1H), 4.0 (d, 1H), 3.69 (d, 1H), 3.47-3.38 (m, 5H), 3.28 (d, 1H), 2.71 (t, 1H), 2.55 (t, 1H), 2.04 (t, 2H), 1.68 (m, 2H), 1.44 (s, 18H), 1.42 (s, 9H), 1.31-1.25 (m, 4H). ^{13}C NMR (125.7 MHZ, CD_3Cl, δ from TMS): 171.95, 171.66, 139.91, 129.35, 128.05, 126.82, 80.30, 63.39, 59.95, 54.79, 53.18, 52.62, 29.41, 28.14, 28.12, 25.83, 25.68. ESI-MS: *m/z* = 547.0 $[M+H]^+$; calcd.: 547.4.

***N,N,N'-trans*-1,2-diaminocyclohexanetri-*tert*-butylacetate (3): 2** (0.757 g, 1.38 mmol) was stirred over Pd/C (96 mg, 13 % by wt.) in MeOH under 1 atm $H_{2(g)}$. After 16 h, the Pd/C was removed by filtration and the

mother liquor concentrated to **3** (601 mg, 1.32 mmol, 95%) as a beige oil. ^{1}H NMR (500 MHZ, $CDCl_3$, δ from TMS): 3.49-3.23 (m, 7H), 2.35 (m, 2H), 2.00 (m, 1H), 1.93 (m, 1H), 1.72 (m, 1H), 1.65 (m, 1H), 1.44 (s, 27H), 1.18-1.00 (m, 4H). ^{13}CNMR (125.7 MHZ, CD_3Cl, δ from TMS): 171.7 (two coincidental C), 80.6, 80.5, 67.3, 57.6, 52.8, 48.7, 31.4, 28.3, 28.2, 27.1, 25.9, 24.5. ESI-MS: *m/z* = 457.3 $[M+H]^+$; calcd.: 457.3.

***N*-(2-picolyl)-*N,N',N'-trans*-l,2-cyclohexylenediaminetri-*tert*-butylacetate (4):** Picolyl chloride hydrochloride (0.079 g, 0.48 mmol) was added to **3** (0.25 g, 0.55 mmol), potassium iodide (0.076 g, 0.48 mmol) and diisopropylethylamine (0.320 g, 2.48 mmol) stirring in 3 mL DMF. After 16 h stirring, the pale yellow and cloudy solution was diluted with 50 mL Et_2O, washed with satd. $K_2CO_{3(aq)}$, copious water and brine, dried over Na_2SO_4 and concentrated to 0.303 g of tan oil. The crude product was purified by flash chromatography (silica gel, 9:1 hexane:EtOAc w/ 1 % TEA) to yield **4** (0.15 g, 0.27 mmol, 50%) as a colorless oil. ^{1}H NMR (500 MHZ, $CDCl_3$, δ from TMS): 8.46 (d, 1H), 7.86 (d, 1H), 7.64 (t, 1H), 7.11 (m, 1H), 4.11 (d, 1H), 3.79 (d, 1H), 3.48-3.32 (m, 5H), 3.29 (d, 1H), 2.71 (m, 1H), 2.61-2.52 (m, 2H), 2.06 (m, 2H), 1.69 (m, 2H), 1.40 (s, 27H), 1.32-1.24 (m, 3H). ^{13}C NMR (125.7 MHZ, CD_3Cl, δ from TMS): 171.8, 166.2, 162.5, 146.8, 137.3, 127.0, 123.5, 80.4 (two coincidental signals), 66.6, 63.3, 62.8, 59.0, 37.4, 291, 28.3, 28.1, 26.0, 24.9, 22.7. ESI-MS: *m/z* = 548.4 $[M+H]^+$; calcd: 548.4.

***N*-picolyl-*N,N',N'-trans*-l,2-cyclohexylenediaminetriacetate trifluoroacetic acid (PyC3A•TFA): 4** (150 mg, 0.27 mmol) was stirred in 5 mL each CH_2Cl_2/TFA. After 12 h, the solution was concentrated to PyC3A•TFA (0.21 mmol, 78%) as 104 mg white solids. pH-potentiometric analysis of the isolated ligand product revealed 4 ionizable protons. Dividing the mass of the titrand by moles hydroxide required to consume each proton yields product MW = 493 (MW PyC3A•TFA = 493.44 g/mol). ^{1}H NMR (500 MHZ, D_2O, 70ºC, δ from protio solvent): 9.35 (br s, 1H), 9.15 (s, 1H), 8.69 (br s, 1H), 8.58 (br s, 1H), 4.93 (br m, 1H), 4.70 (br m, 1H), 4.55-4.3 (br m, 3H), 4.16-4.09 (br m, 2H), 3.62 (br s, 1H), 2.82 (br m 2H), 2.46 (br s, 2H), 2.05 (br s, 2H), 1.90 (br s, 2H). ^{13}C NMR (125.7 MHZ, D_2O, 70ºC, δ from dioxane): 174.8, 169.3, 153.0, 148.0, 142.4, 127.9, 127.0, 64.9, 62.0, 53.3, 52.7, 52.4, 24.6 (two coincidental signals), 24.5, 24.3. ^{19}F NMR (470.1 MHZ, D_2O, δ from potassium fluoride): 173.9. ESI: *m/z* = 380.2 $[M+H]^+$; calcd: 379.2.

Na[Mn(PyC3A)(H_2O)]: PyC3A•TFA (0.038g 70.0 μmol) and $MnCl_2$•$4H_2O$ (0.020g, 101 μmol) were combined in 5 mL H_2O and the pH adjusted to 6.5. The mixture was purified by RP-HPLC using the C18 column and method P2. The fractions containing pure product were freeze dried to yield pure $[Mn(PyC3A)(H_2O)]^-$ as a white solids (0.021g, 44.5 μmol. 57.7%). Solutions of $[Mn(PyC3A)(H_2O)]^-$ could be prepared in situ. $MnCl_2$ was titrated into buffered solutions of PyC3A•TFA and complex formation was monitored by LC-MS (to check for any free chelate) and T_2 ^{1}H NMR (any excess Mn(II) results in a sharp r_2

increase:)[8] final Mn concentrations were confirmed by ICP-MS. ESI: *m/z* = 433.1 $[M+2H]^+$; calcd. 433.1. m/z = $[431.0]^-$; calcd: $[431.1]^-$.

***N*-(6-methyl)-methylnicatinoyl-*N,N',N'-trans*-l,2-cyclohexylenediaminetri-*tert*-butylacetate (6)**. 6-(bromomethyl)-methylnicatinoate (0.450 g, 1.95 mmol) was added to **3** (1.00 g, 2.01 mmol), potassium iodide (0.243 g, 1.46 mmol), and diisopropylethylamine (0.468 g, 3.62 mmol) stirring in 4 mL DMF. After 3h, the reaction was diluted to 100 mL with Et_2O, washed with satd. $Na_2CO_{3(aq)}$, copious water and brine before drying over Na_2SO_4 and concentration to a brown oil. The crude product was purified by flash chromatography (basic alumina, hexane:EtOAc, 0% to 20% EtOAc) and as 1.02 g (1.68 mmol, 84%) **6** was isolated as a clear colored oil. ^{1}H NMR (500 MHZ, $CDCl_3$, δ from protio solvent): 9.07 (s, 1H), 8.24 (d, 1H), 8.03 (d, 1H), 4.20 (d, 1H), 3.04 (s, 3H), 3.86 (d, 1H), 3.53-3.30 (m, 6H), 2.73 (br t, 1H), 2.58 (br t, 1H), 2.05 (br m, 2H), 1.69 (br m, 2H), 1.65 (br m, 2H), 1.45 (s, 18H), 1.43 (s, 9H), 1.26-1.09 (m, 4H). ^{13}C NMR (125.7 MHZ, $CDCl_3$, δ from protio solvent): 171.8, 171.7, 166.4, 166.3, 149.9, 137.5, 124.3, 123.7, 80.7, 80.6, 63.7, 62.0, 56.4, 54.0, 53.0, 52.4, 28.3, 26.0, 25.9. ESI-MS: *m/z* = 606.4 $[M+H]^+$; calcd: 606.4.

N'-(6-methyl)nicatinoyl-,N',N'',N''trans-l,2-cyclohexylenediaminetri-^{t}Bu-acetate (7): Lithium hydroxide (0.044 g, 1.84 mmol) and **6** (1.02 g, 1.69 mmol) were combined in 16 mL of 1:1 THF:H_2O and stirred for 3h at RT. The reaction was then concentrated to dryness and purified by preparative RP-HPLC using the C18 column and method P1. Fractions containing pure product were freeze dried to yield product as a white solid (0.670 g, 1.13 mmol, 67%). ^{1}H NMR (500 MHZ, D_2O, δ from protio solvent, stirred over K_2CO_3(s)): 9.09 (s, 1H), 8.15 (d, 1H), 7.07 (d, 1H), 3.95 (d, 1H), 3.63 (d, 1H), 3.28 (d, 1H), 3.14-3.06 (m, 5H), 2.33 (br t, 2H), 1.94 (m, 2H), 1.68 (m, 2H), 1.43 (9H), 1.38 (18H), 1.18-0.99 (m, 4H). ^{13}C NMR (125.7 MHZ, $CDCl_3$, δ from protio solvent, stirred over K_2CO_3(s))): 172.2, 171.9, 170.8, 158.2, 151.1, 1380, 131.1, 122.9, 81.8, 81.5, 62.1, 59.5, 55.9, 53.0, 52.6, 29.8, 28.1, 28.0, 25.9, 25.7, 25.4, 24.8. ESI-MS: *m/z* = 592.3 $[M+H]^+$; calcd: 592.4.

***N*-(6-methyl)-N-hydoxysuccinimidylnicatinoyl-,*N*,*N*',*N*'-*trans*-l,2-cyclohexylenediaminetri-*tert*-butylacetate (^{t}Bu-PyC3A-NHS)**. (0.471 g, 0.797 mmol) **7** was stirred with dicyclohexylcarbodiimide (0.167 g, 0.809 mmol) and N-hydroxysuccinimide (0.109 g, 0.947 mmol) in 10 mL THF. A white precipitate formed within seconds. LC-MS confirmed full conversion after 16 h stirring. The precipitate was removed by filtration and the clear mother liquor concentration to a pale, colorless oil. The product can be carried directly through to the next step, or purified by RP-HPLC using the C18 column and method P1**.** ^{1}H NMR (500 MHZ, D_2O, δ from protio solvent): 9.15 (s, 1H), 8.32 (d, 1H), 8.21 (d, 1H), 4.33 (d, 1H), 4.15 (d, 1H), 3.55-3.25 (m, 6H), 2.91 (s, 4H), 2.73 (t, 1H), 2.50 (t, 1H), 1.91 (m, 2H), 1.81 (m, 2H), 1.45 (18H), 1.38 (9H), 1.18-1.02 (m 4H). ^{13}C NMR (125.7 MHZ, $CDCl_3$, δ from protio solvent): 171.5, 169.3, 169.2, 161.3, 150.3, 138.2, 124.29, 119.7, 108.0,

98.5, 80.7, 80.6 (two coinicidental peaks), 68.6, 63.9, 62.2, 54.0, 52.8, 49.3, 34.0, 28.2 (two coincidental peaks), 29.3, 25.9, 25.9 (two coincidental peaks), 25.8, 25.7. ESI-MS: *m/z* = 689.3 $[M+H]^+$; calcd: 689.4.

^{t}Bu-protected FBP-CyP3A$_4$ (8): The oil was taken up in 2 mL DMF and added to *L*-2,4-diamino-N-butyramide-[Tyr-dGlu-Cys-Hyp-Typ(3-Cl)-Leu-Cys-Ile-Gln (3→8) disulfide]-1-(4-[(*L*-2,4-diamino-butyrylamino)-methyl]-benzylamide (EP2104/24: 0.211 g, 0.123 mmol)) and 4-dimethylaminopyridine (0.016g, 0.131 mmol) stirring in 2 mL DMF. The reaction was adjusted to pH 6.5 with DIPEA and stirred at RT. After 16 h stirring, 250 mL satd. NaCl solution was added to the reaction mixture dropwise to precipitate white solids. ^{t}Bu-protected FBP-CyP3A$_4$ was purified by RP-HPLC using the C5 column and method P3. Fractions containing product were freeze dried to yield product as a white solid (0.177g, 0.0441 mmol, 35 %). ESI-MS: *m/4z* = 1004.0 $[M+4H]^{4+}$; calcd. 1004.0. *m/3z* = 1338.4 $[M+3H]^{3+}$; calcd. 1338.4. *m/2z* = 2007.6 $[M+2H]^{2+}$; calcd. 2007.6.

FBP-CyP3A$_4$ (9): Compound **8** (0.177g, 44.1 µmol) was stirred in 5 mL of a 91:3:3:3 mixture of TFA: methane sulfonic acid: n-dodecanethiol: water for 90 min before dilution with 50 mL Et_2O. The flocculent white solids were centrifuged to a solid pellet and the supernatant decanted. After several washes with Et_2O the solids were dried to yield pure product as a white powder (0.147 g, 44.0 µmol, 100%). ESI-MS: *m/3z* = 1113.6 $[M+3H]^{3+}$; calcd. 1113.8. ESI-MS: *m/z* = 1670.1 $[M+2H]^{3+}$; calcd. 1670.2.

Mn-FBP: The pH of a 10 mL solution of FBP-CyP3A$_4$ (0.018 g, 5.4 µmol) adjusted to pH 6.5 was added $MnCl_2$*$4H_2O$ (0.0053 g, 27.0 µmol). The solution was re-adjusted to pH 6.5 and purified by RP-HPLC using the C5 column and method P2. Fractions containing product were freeze dried to yield pure product as a while powder (0.0080 g, 2.2 µmol, 41%). ESI-MS: *m/3z* = 1184.6 $[M+8H]^{3+}$; calcd. 1184.4. *m/2z* = 1776.4 $[M+6H]^{2+}$; calcd. 1776.5.

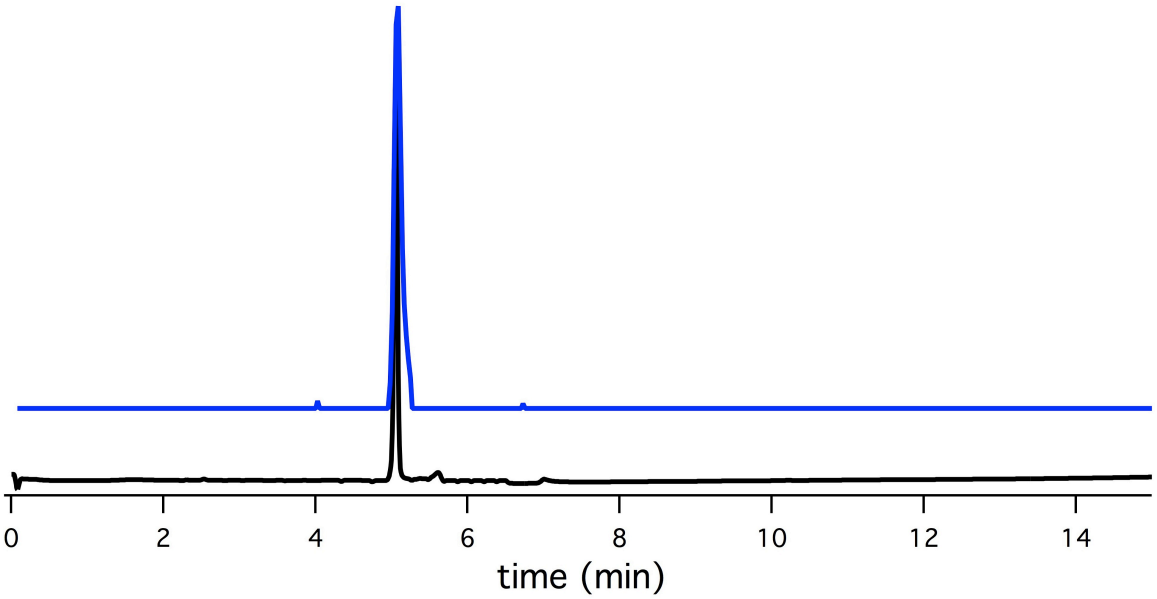

Figure S1. LC trace of PyC3A at 254 nm detection (black) and MS chromatogram of extracted m/z^+ 380 (method A1).

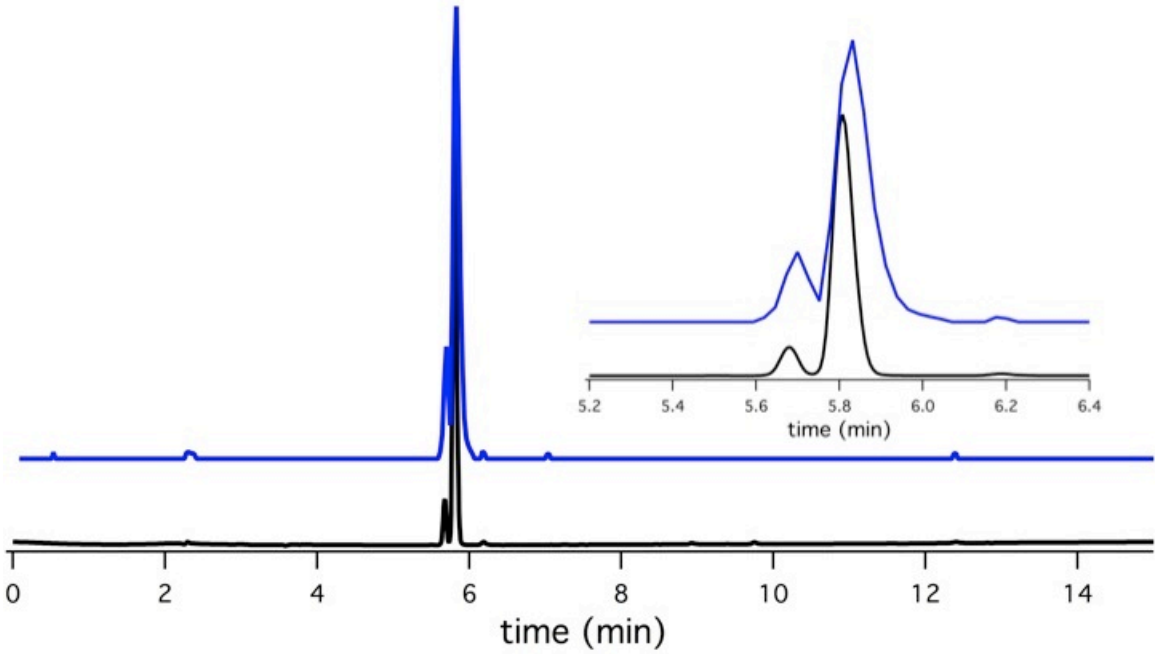

Figure S2. LC trace of $[Mn(PyC3A)(H_2O)]^-$ at 254 nm detection (black) and MS chromatogram of extracted m/z^- 431. Inset zoom depicts chromatographically resolved diastereomers (method A2).

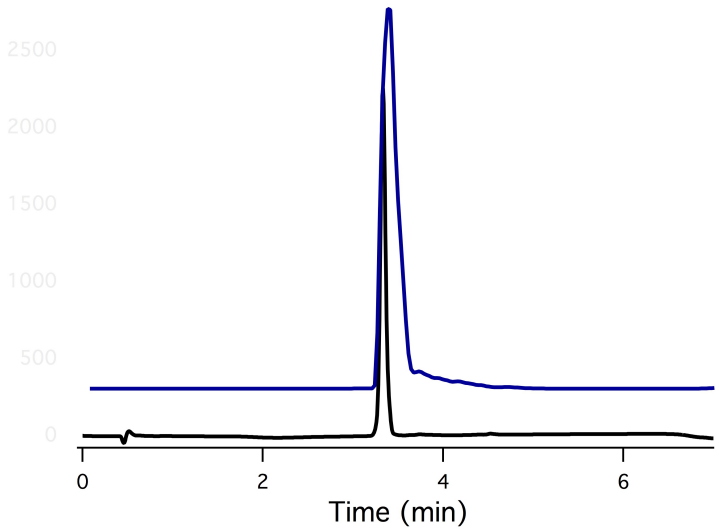

Figure S3. LC trace of ^{t}Bu-PyC3A-NHS at 254 nm detection (black) and MS chromatogram of extracted m/z^{+}689.

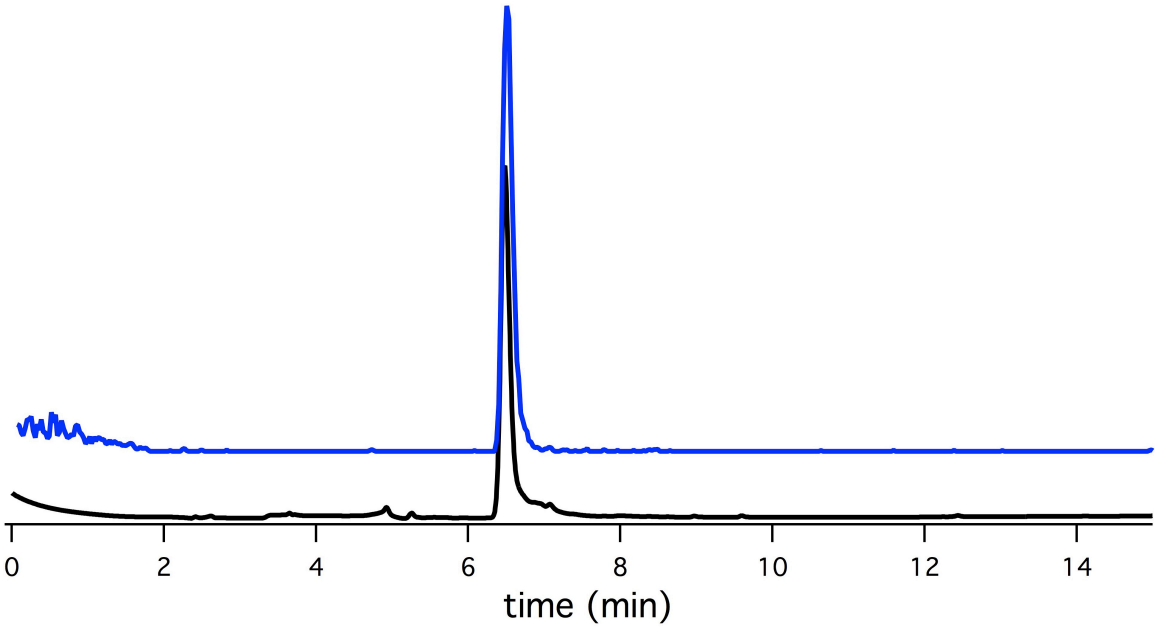

Figure S4. LC trace of **9** at 254 nm detection (black) and MS chromatogram of extracted $m/3z^{+}$ 1114 (method A2).

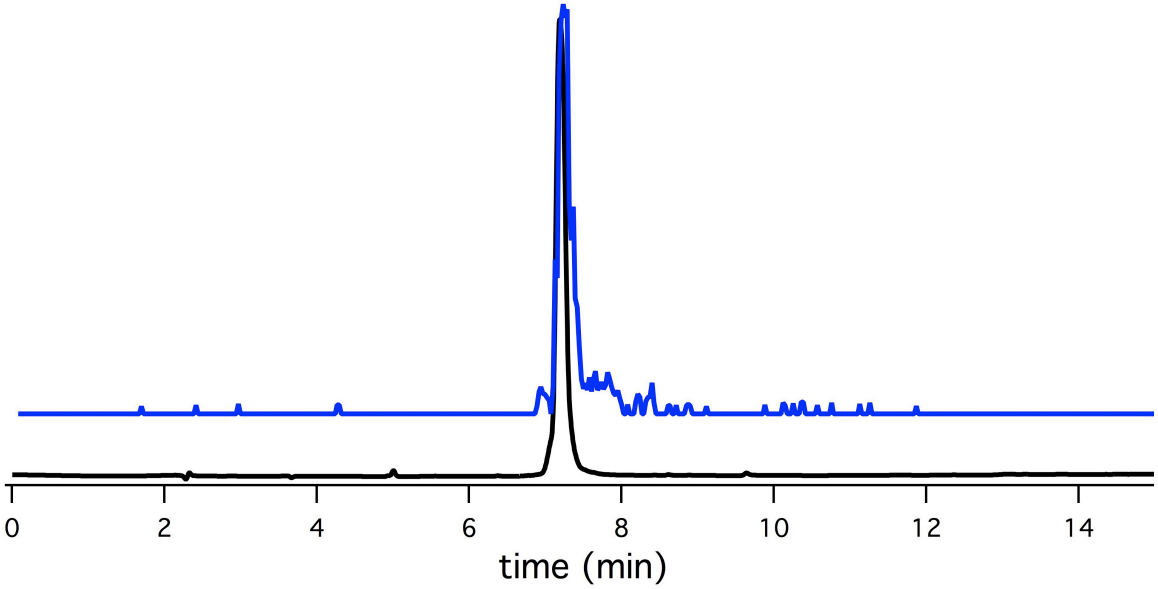

Figure S5. LC trace of Mn-FBP at 254 nm detection (black) and MS chromatogram of extracted $m/3z^+$ 1184 (method A2).

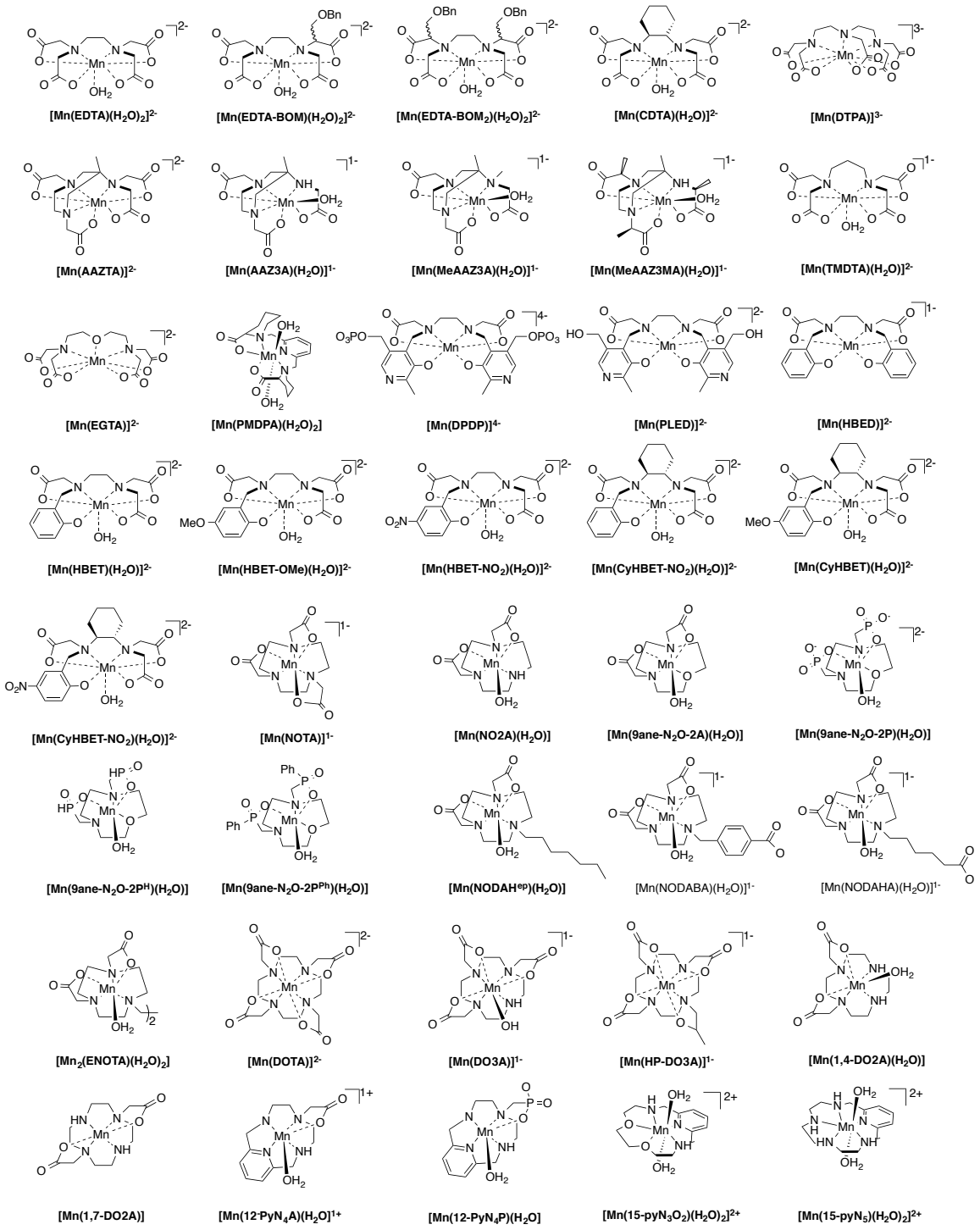

Figure S6. Mn(II) complexes considered for comparison to $[Mn(PyC3A)(H_2O)]^-$.

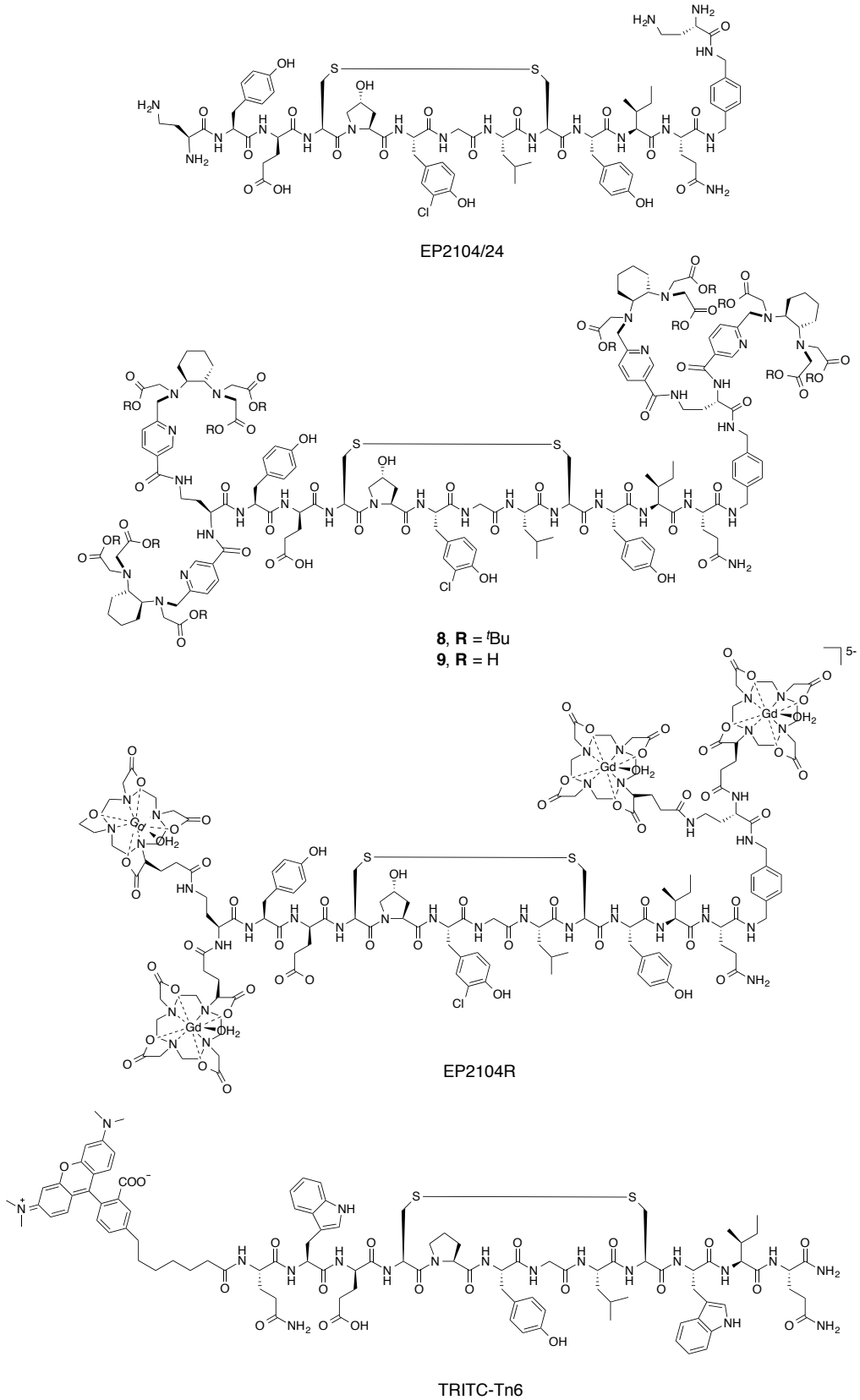

Figure S7. Fibrin binding peptide derivatives discussed but not depicted in main text.

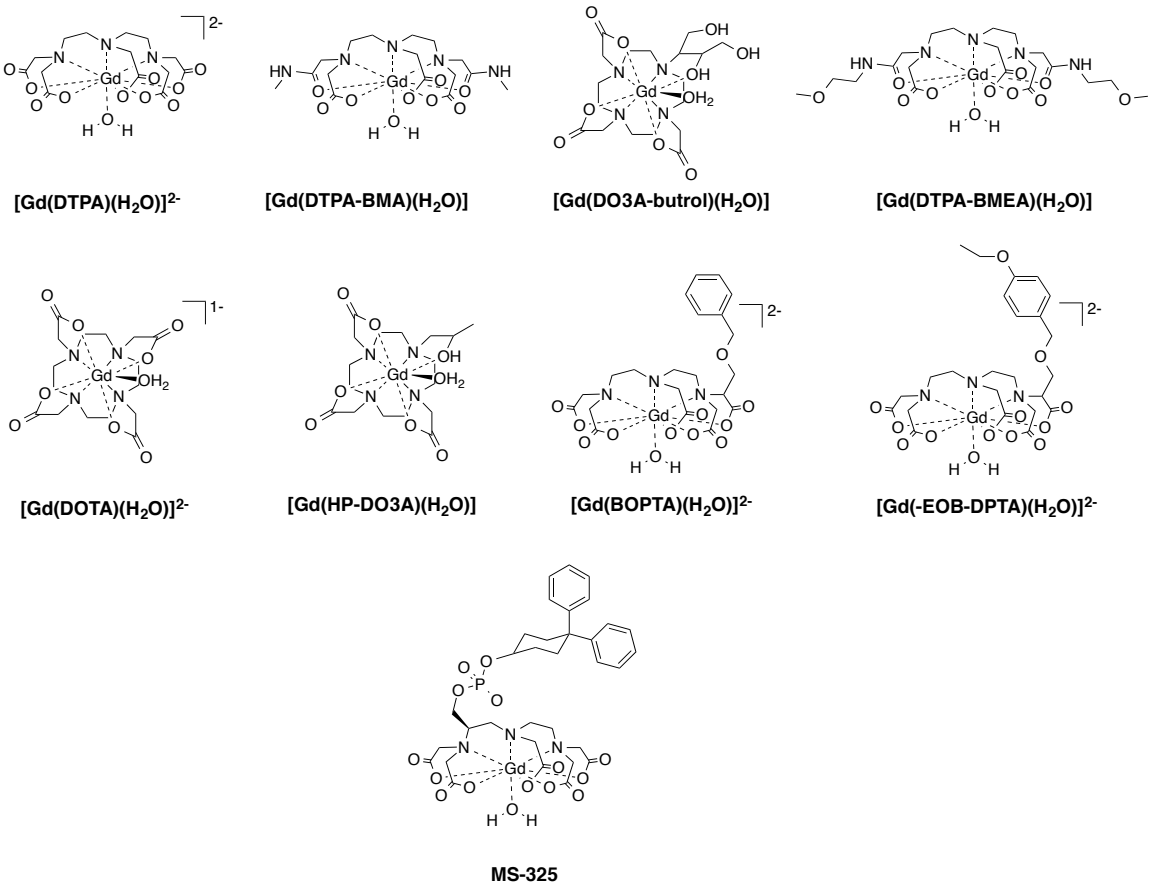

Figure S8. Gd-based imaging probes discussed in main text and Table S3.

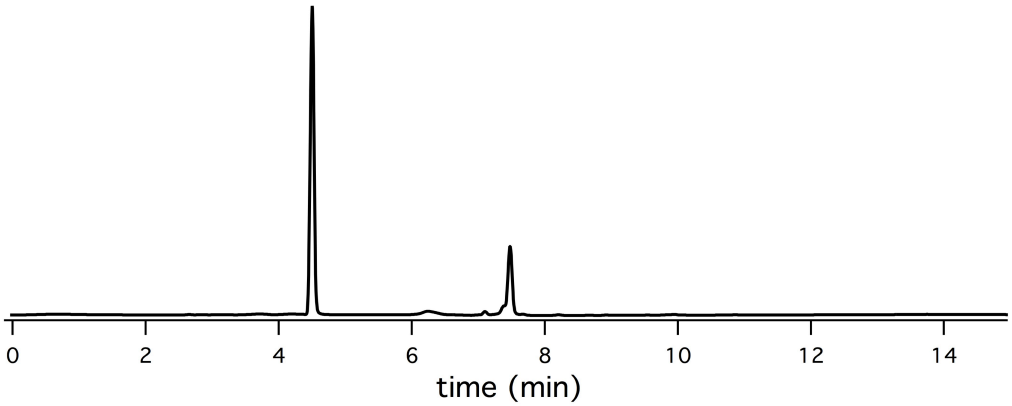

Figure S9. LC trace (254 nm detection, method A2)) of equilibrium mixture following addition of CDTA to $[Mn(PyC3A)(H_2O)]^-$ at pH 7.4. Peaks at 4.4 and 7.5 min correspond to free PyC3A and $[Mn(PyC3A)(H_2O)]^-$, respectively.

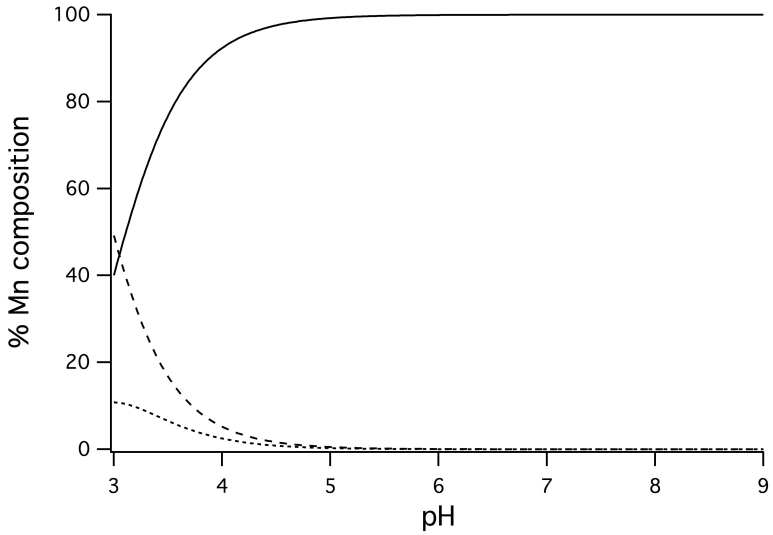

Figure S10. %Mn composition in mixture of 1 mM each Mn(II) and PyC3A at 25 °C, 0.15M NaCl. ML, MLH and free M are represented by the solid, dotted and dashed traces, respectively.

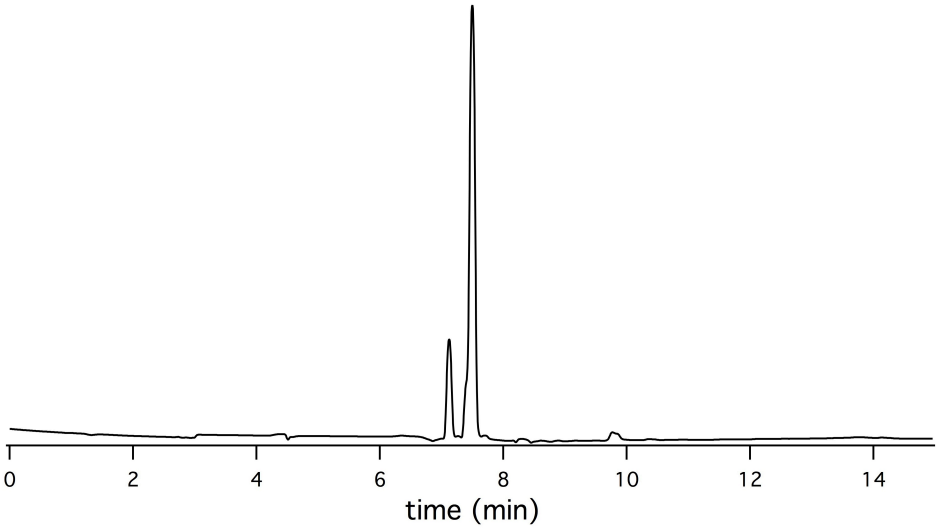

Figure S11. LC trace (254 nm detection, method A2) of mixture containing 2.5 mM $[Mn(PyC3A)(H_2O)]^-$ and 2.5 mM $ZnPO_4$ in 50 mM phosphate buffer, at pH 7.0 after 70 min incubation at 37 °C. Peaks at 7.1 and 7.5 correspond to $[Zn(PyC3A)]^-$ and $[Mn(PyC3A)(H_2O)]^-$, respectively

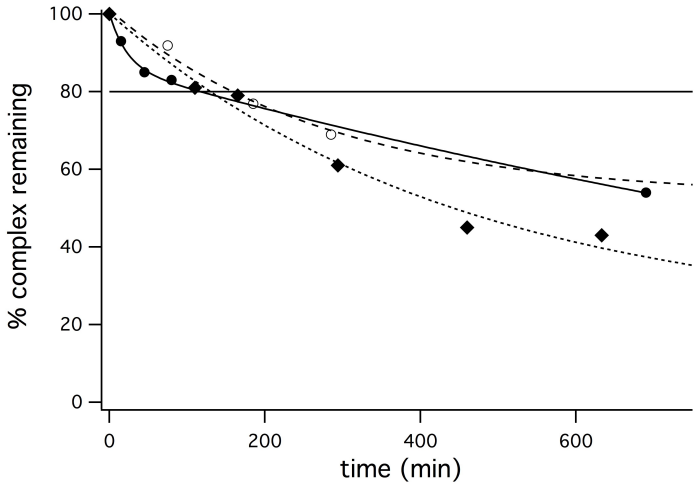

Figure S12. Zn assisted displacement of Gd or Mn from $[Mn(PyC3A)(H_2O)]^{2-}$ (filled circles), $[Gd(DTPA)(H_2O)]^{2-}$ (open circles) and [Gd(DTPA-BMA)(H_2O)] (filled diamonds) as a function of time. 2.5 mM imaging probe, 2.5 mM $Zn(OTf)_2$, 50 mM pH 7.0 phosphate buffer, 37 °C.

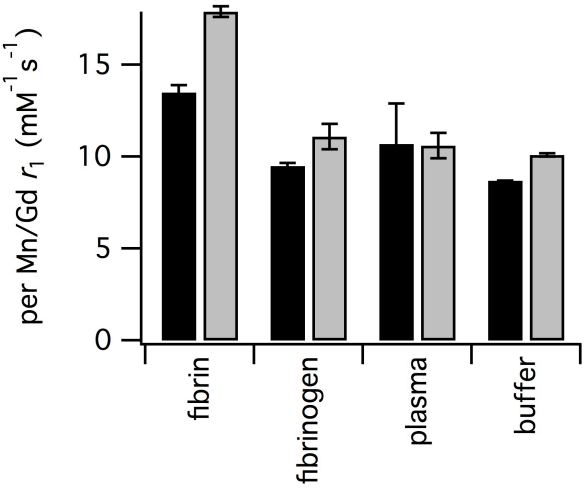

Figure S13. Relaxivity of Mn-FBP (black) and EP2104R (grey) in the presence of pH 7.4 buffer, bovine blood plasma, human fibrinogen, and human fibrin gel at 1.4T, 37 ºC.

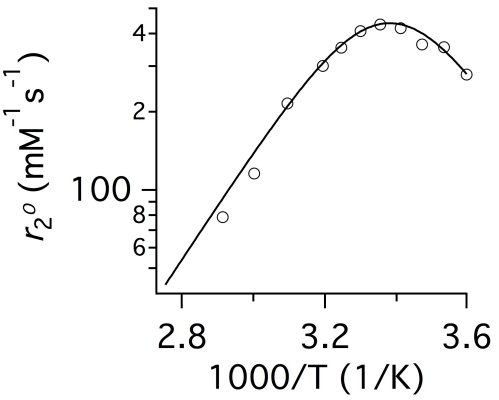

Figure S14. $H_2{}^{17}O$ tranverse relaxivity in the presence of Mn-FBP (open circles) as a function of temperature. Solid lines are fits to the data.

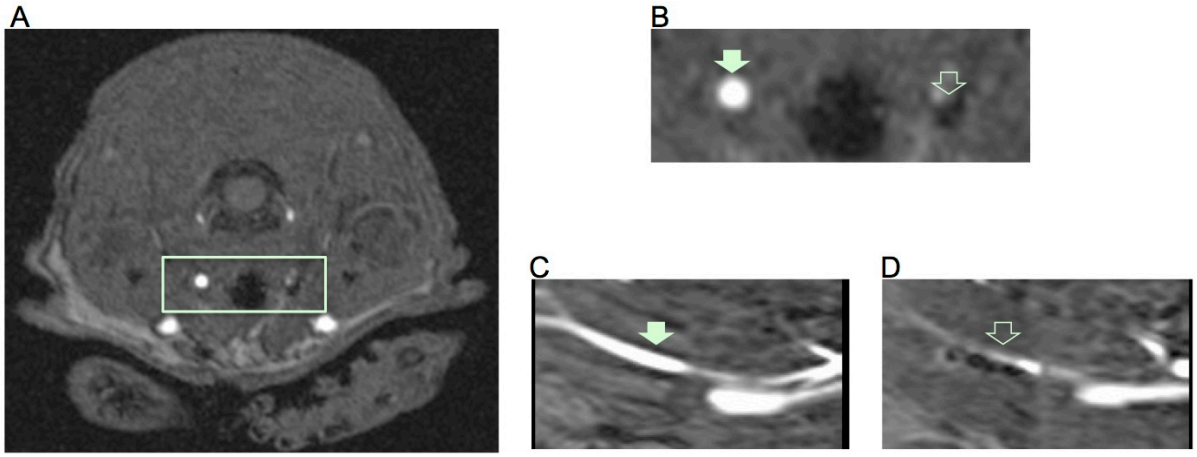

Figure S15. TOF angiogram depicting flow deficit in the right carotid artery of the rat model. (A) Axial slice at the level of thrombus; (B) expansion of the boxed region in (A), right coratid artery denoted with empty arrow, contralateral vessel depicted with filled arrow; (C) sagittal slice at the level of the contralateral vessel; (D) sagittal slice at the level of the thrombus.

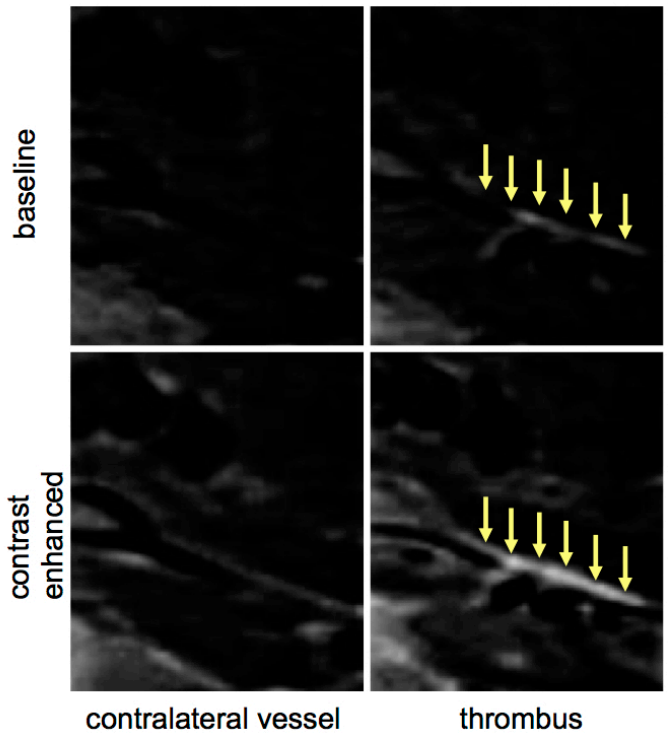

Figure S16. Sagittal slices from 3-dimensional T_1-weighted image in rat model with arterial blood suppression at the level of thrombus (denoted by arrows) and contralateral vessel taken at baseline and 35 min following administration of Mn-FBP.

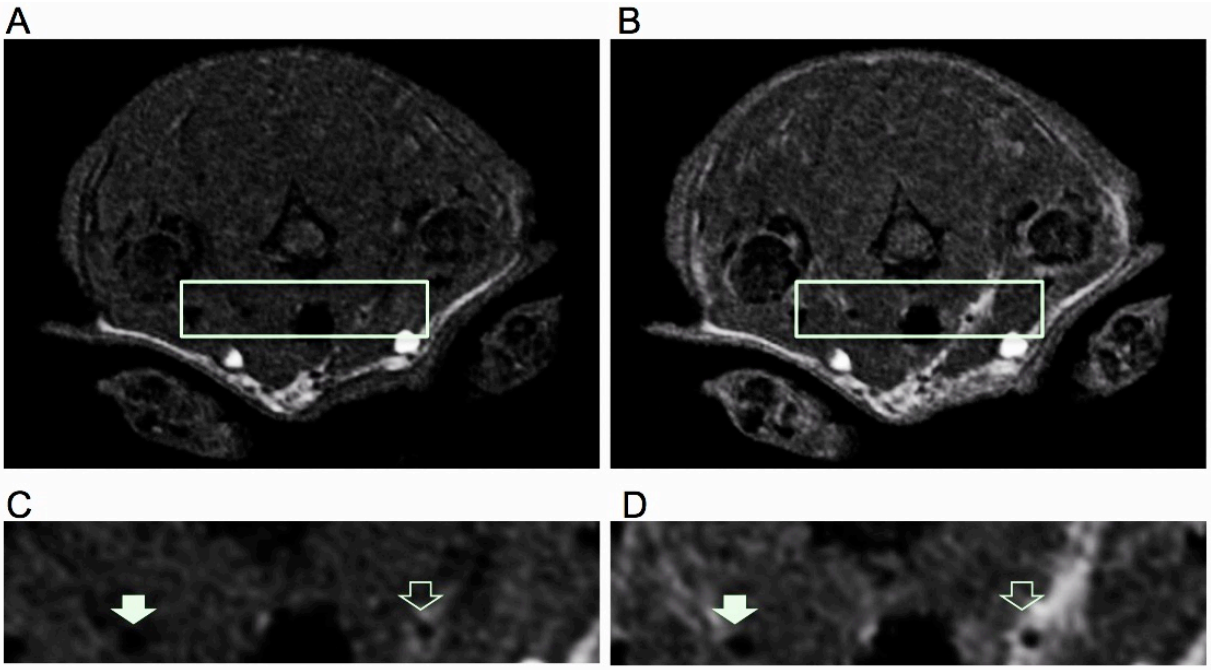

Figure S17. MR data acquired following administration of EP2104R to rats. (A and B) Axial slices from 3-dimensional T_1-weighted MRI with arterial blood suppression at the level of the thrombus acquired at baseline and 35 min after administration of EP2104R, respectively. (C and D) The regions inside the boxes in (A) and (B) are expanded, respectively. The thrombus is denoted with the open arrow and the contralateral vessel with the filled arrow.

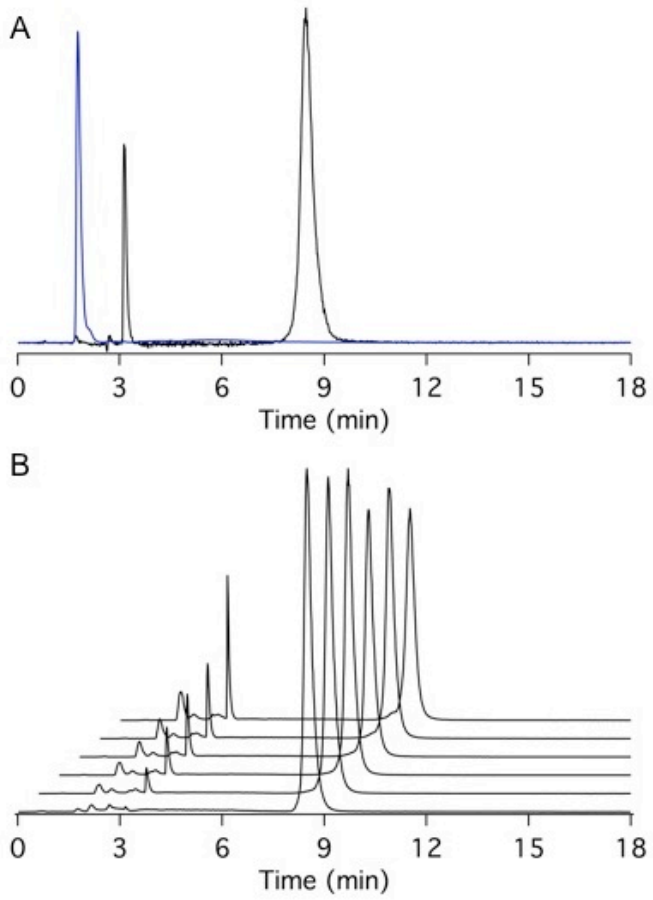

Figure S18. (A) LC-ICP-MS traces of plasma analyzed for Mn from blood drawn 15 min after intravenous Mn-FBP injection (black trace) and $MnCl_2$ in blood plasma (blue trace). (B) LC-ICP-MS traces analyzed for Mn from a solution of Mn-FBP incubated in rat plasma at 37 ºC for 0, 1, 2, 3, 4, and 9h (front to back). The chelated Mn metabolite (3.1 min) observed in vivo also appears after incubation of Mn-FBP (8.5 min) in blood plasma.

	log K_{ML}	log $K_{ML\ pH\ 7.4}$	pMn[a]
		Rationally Designed Chelate, q = 1	
PyC3A	13.86[b]	11.34[b], 11.40[c]	8.06[b]
		Acyclic Chelates, *q* < 1	
AAZTA[9]	14.19[b]	11.31[b]	8.15[b]
DTPA[10]	14.54[b]	10.93[b]	7.77[b]
EGTA[10]	11.60[b]	8.82[b]	6.91[b]
AAZ3A[9]	11.00[b]	8.15[b]	6.58[b]
AAZ3MA[9]	10.67[b]	7.77[b]	6.39[b]
BIMP[10]	9.74[b]	7.57[b]	6.30[b]
MeAAZ3A[9]	11.43[b]	7.03[b]	6.47[b]
PMDPA[11]	11.37[f]	6.82[f]	5.94[f]
TMDTA[10]	9.70[b]	6.54[b]	5.81[b]
DPDP[12]	15.10[d]	6.33[d]	5.72[d]
HBED[12]	14.78[d]	6.33[d]	5.72[d]
PLED[12]	12.56[d]	6.09[d]	5.61[d]
		Acylcic Chelates, *q* ≥ 1	
CyDTA[10,13]	14.32[b], 14.69[d]	12.34[b], 12.64[d]	8.67[b], 8.82[d]
EDTA-BOM_2[14]	13.90[e]	11.02[e]	8.12[e]
EDTA-BOM[14]	13.50[e]	10.62[e]	7.82[e]
EDTA[10,13,14]	12.46[b], 12.61[d], 13.88[e]	10.49[b], 10.67[d], 11.02[e]	7.82[b], 7.83[d], 8.01[e]
CyHBET-NO_2[13]	13.66[d]	10.10[d]	7.55[d]
HBET-NO_2[13]	11.29[d]	8.73[d]	7.01[d]
HBET[13]	13.07[d]	7.97[d]	6.62[d]
HBET-OMe[13]	13.32[d]	7.91[d]	6.48[d]
CyHBET[13]	14.16[d]	7.76[d]	6.68[d]
CyHBET-OMe[13]	14.61[d]	6.95[d]	6.24[d]
		Macrocyclic Chelates, *q* < 1	
DOTA[15]	19.89[g]	13.27[g]	8.94[g]
DO3A[15]	19.49[g]	12.25[g]	8.62[g]
HPDO3A[15]	17.89[g]	12.18[g]	8.59[g]
NOTA[16,17]	14.90[g], 16.3[g]	10.88[g], 10.52[g]	7.94[g], 7.76[g]
1,4-DO2A[15]	16.13[g]	10.10[g]	7.55[g]
1,7-DO2A[15]	14.54[g]	8.21[g]	6.61[g]
		Macrocylic Chelators, *q* ≥ 1	
15-pyN_5[18]	10.89[g]	7.72[g]	6.37[g]
12-pyN_4P[19]	14.06[g]	7.35[g]	6.19[g]
12-pyN_4A[19]	11.54[g]	7.14[g]	6.09[g]
NO2A[20]	11.56[h]	7.11[h]	5.96[h]
NODAHA[21]	10.15[f]	6.43[f]	5.76[f]
NODAH[ep 21]	10.98[f]	6.37[f]	5.73[f]

NODABA[21]	9.90[f]	6.10[f]	5.61[f]
15-pyN_3O_2[18]	7.18[g]	5.20[g]	5.27[g]
9-aneN_2O-2P[20]	10.61[g]	5.07[g]	5.23[g]
9-aneN_2O-2A[20]	7.43[g]	4.36[g]	5.06[g]
9-aneN_2O-2P^{H}[20]	4.30[g]	3.34[g]	5.01[g]
9-aneN_2O-2P^{Ph}[20]	4.82[g]	2.98[g]	5.00[g]

Table S1. Comparison of formation constants of Mn complexes formed with PyC3A and previously studied chelates. In each group, chelates are ordered by conditional logK_{ML} at pH 7.4. [a]pMn at 10 μM MnL, pH 7.4; [b]*I* = 0.15 M NaCl, 25 °C; [c]determined from K_{comp} with CDTA challenge, pH 7.4 Tris 50 mM, RT; [d]*I* = 0.10 M NaCl, 25 °C; [e]*I* = 1.0 M KCl, 25 °C; [f]*I* = 0.1 M KCl, 25 °C; [g]*I* = 0.1 M Me_4NCl, 25 °C; [h]*I* = 0.1 M $NaNO_3$, 25 °C.

	r_1^{298} ($mM^{-1}s^{-1}$)	r_2^{298} ($mM^{-1}s^{-1}$)	r_1^{310} ($mM^{-1}s^{-1}$)	r_2^{310} ($mM^{-1}s^{-1}$)	q	k_{ex}^{310} ($x10^7$ s^{-1})	$\Delta H^{\neq}$	$A_o/\hbar$
PyC3A	2.8[a], 3.3[b]	--	2.1[a], 2.5[b]	4.9[a]	1	11	37.2	2.87
EDTA[14]	3.0[c]	--	2.2[a,d]	3.7[a,d]	1	59	36.7	3.79
EDTA-BOM[14]	3.6[b]	--	--	--	1	19	43.1	3.79
EDTA-BOM_2[14]	4.3[b]	--	--	--	1	25	38.4	3.79
EDTA-Tyriso[8]	--	--	3.2[a], 3.6[b]		1	30	35.6	2.92
Mn-453car[2,22]	5.8[b]	--	--	--	0.8	30	21.1	3.33
CDTA[2]	--	--	2.1[a,d]	3.5[a,d]	1	27	35.8	3.14
AAZTA[9]	1.6[b9]	--	--	--	0	--	--	--
AAZ3A[9]	2.5[b]	--	--	--	0<q<1	7.0	22.8	--
MeAAZ3A[9]	2.0[b]	--	--	--	0<q<1	20	26.5	--
AAZ3MA[9]	1.9[b]	--	--	--	0<q<1	18	16.7	--
HBET[13]	--	--	2.8[a]	9.4[a]	1	370	33.8	3.54
HBET-OMe[13]	--	--	3.1[a]	11.1[a]	1	360	40.7	4.15
HBET-NO_2[13]	--	--	2.3[a]	4.8[a]	0.5	48	41.2	3.48
CyHBET[13]	--	--	3.3[a]	6.0[a]	1	770	41.2	3.36
CyHBET-OMe[13]	--	--	3.3[a]	5.8[a]	1	300	20.7	4.02
CyHBET-NO_2[13]	--	--	2.3[a]	3.7[a]	1	190	31.3	3.97
ENOTA[23]	3.4[b]	--	2.7[b]	--	1	7.9	20.5	3.27
9-aneN_2O-2A[20]	2.8[b]	--	2.3[b]	--	1	2.3	38.8	3.33
9-aneN_2O-2P[20]	5.1[b]	--	4.3[b]	--	1	140	11.7	3.33
1,4-DO2A[24]	2.1[b]	--	--	--	0<q<1	110	29.4	4.10
1,7-DO2A[24]	1.5[b]	--	--	--	0	--	--	--
DO1A[24]	2.4[b]	--	--	--	1	500	17.6	3.94
12-pyN_4A[19]	2.4[b]	--	1.9[b]	--	1	330	13.0	3.66
12-pyN_4P[19]	2.8[b]	--	2.3[b]	--	1	250	14.0	3.99
15-pyN_5[18]	4.5[b]	--	3.6[b]	--	2	13	37.7	3.86
15-pyN_3O_2[18]	3.6[b]	--	3.1[b]	--	2	0.69	35.3	3.86
15-pyN_5[18]	4.5[b]	--	3.6[b]	--	2	13	37.7	3.86

Table S2. Comparison of r_1, r_2, hydration state (q), water exchange rate (k_{ex}) and enthalpy of activation of water exchange ($\Delta H^{\neq}$) in water for $[Mn(CyP3A)(H_2O)]^-$ and previously reported Mn complexes. [a]1.4 T; [b]0.47 T; [c]0.56 T. [d]This study.

	r_1 ($mM^{-1}s^{-1}$)	r_2 ($mM^{-1}s^{-1}$)
$[Mn(PyC3A)(H_2O)]^{-}$ [a]	3.8	7.6
$[Gd(DTPA)(H_2O)]^{2-}$	4.1	4.6
[Gd(DO3A-butrol)]	5.2	6.1
$[Gd(HP\text{-}DO3A)(H_2O)]$	5.1	5.0
$[Gd(BOPTA)(H_2O)]^{2-}$	6.3	8.7
$[Gd(DOTA)(H_2O)]^{-}$	3.6	4.3
$[Gd(DTPA\text{-}BMA)(H_2O)]$	4.3	5.2
$[Mn(DPDP)]^{4-}$	3.6	7.1
$[Gd(EOB\text{-}DTPA)(H_2O)^{2-}$	6.9	8.7
MS-325	19	34

Table S3. Comparison of 1.5T relaxivity[25] of $[Mn(PyC3A)(H_2O)]^{-}$ to clinically used MR imaging probes in bovine plasma at 37 °C. [a]Recorded at 1.4T.

References

(1) Fulmer, G. R.; Miller, A. J. M.; Sherden, N. H.; Gottlieb, H. E.; Nudelman, A.; Stoltz, B. M.; Bercaw, J. E.; Goldberg, K. I. *Organometallics* **2010**, *29*, 2176.

(2) Gale, E. M.; Zhu, J.; Caravan, P. *J. Am. Chem. Soc.* **2013**, *135*, 18600.

(3) Overoye-Chan, K.; Koerner, S.; Looby, R. J.; Kolodziej, A. F.; Zech, S. G.; Deng, Q.; Chasse, J. M.; McMurry, T. J.; Caravan, P. *J. Am. Chem. Soc.* **2008**, *130*, 6025.

(4) Gans, P.; Sabatini, A.; Vacca, A. *Talanta* **1996**, *1996*, 1739.

(5) Kolodziej, A. F.; Nair, S. A.; Graham, P.; McMurry, T. J.; Ladner, R. C.; Wescott, C.; Sexton, D. J.; Caravan, P. *Bioconjugate Chem.* **2012**, *23*, 548.

(6) Health, N. I. o. *Guide for the care and use of laboratory animals* Bethesda, MD, 1985.

(7) Drewry, J. A.; Fletcher, S.; Hassan, H.; Gunning, P. T. *Org. Biomol. Chem.* **2009**, *7*, 5074.

(8) Zhu, J.; Gale, E. M.; Atanasova, I.; Rietz, T. A.; Caravan, P. *Chem. Eur. J.* **2014**, *20*, 14507.

(9) Tei, L.; Gugliotta, G.; Fekete, M.; Kálmán, F. K.; Botta, M. *Dalton Trans.* **2011**, *40*, 2025.

(10) Kálmán, F. K.; Tircsó, G. *Inorg. Chem.* **2012**, *51*, 10065.

(11) Su, H.; Wu, C.; Zhu, J.; Miao, T.; Wang, D.; Xia, C.; Zhao, X.; Gong, Q.; Song, B.; Ai, H. *Dalton Trans.* **2012**, *41*, 14480.

(12) Rocklage, S. M.; Cacheris, W. P.; Quay, S. C.; Hahn, F. E.; Raymond, K. N. *Inorg. Chem.* **1989**, *28*, 477.

(13) Gale, E. M.; Mukherjee, S.; Liu, C.; Loving, G. S.; Caravan, P. *Inorg. Chem.* **2014**, *53*, 10748.

(14) Aime, S.; Anelli, P. L.; Botta, M.; Brocchetta, M.; Canton, S.; Fedeli, F.; Gianolio, E.; Terreno, E. *J. Biol. Inorg. Chem.* **2002**, *7*, 58.

(15) Bianchi, A.; Calabi, L.; Giorgi, C.; Losi, P.; Mariani, P.; Palano, D.; Paoli, P.; Rossi, P.; Valtancoli, B. *J. Chem. Soc. Dalton Trans.* **2001**, 917.

(16) Cortes, S.; Brücher, E.; Geraldes, C. F. G. C.; Sherry, A. D. *Inorg. Chem.* **1990**, *29*, 5.

(17) Drahoš, B.; Kubíček, V.; Bonnet, C. S.; Hermann, P.; Lukeš, I.; Tóth, E. *Dalton Trans.* **2011**, *40*, 1945.

(18) Drahoš, B.; Kotek, J.; Hermann, P.; Lukeš, I.; Tóth, E. *Inorg. Chem.* **2010**, *49*, 3224.

(19) Drahoš, B.; Kotek, J.; Císařová, I.; Hermann, P.; Helm, L.; Lukeš, I.; Tóth, E. *Inorg. Chem.* **2011**, *50*, 12785.

(20) Drahoš, B.; Pniok, M.; Havlíčková, J.; Kotek, J.; Císařová, I.; Hermann, P.; Lukeš, I.; Tóth, E. *Dalton Trans.* **2011**, *30*, 10131.

(21) de Sá, A.; Bonnet, C. S.; Geraldes, C. F. G. C.; Tóth, É.; Ferreira, P. M. T.; André, J. P. *Dalton Trans.* **2013**, *42*, 4522.

(22) Troughton, J. S.; Greenfield, M. T.; Greenwood, J. M.; Dumas, S.; Wiethoff, A. J.; Wang, J.; Spiller, M.; McMurry, T. J.; Caravan, P. *Inorg. Chem.* **2004**, *43*, 6313.

(23) Balogh, E.; He, Z.; Hsieh, W.; Liu, S.; Tóth, E. *Inorg. Chem.* **2007**, *46*, 238.

(24) Rolla, G. A.; Platas-Iglesias, C.; Botta, M.; Tei, L.; Helm, L. *Inorg. Chem.* **2013**, *52*, 3268.

(25) Rohrer, M.; Bauer, H.; Mintorovitch, J.; Requardt, M.; Weinmann, H.-J. *Invest. Radiol.* **2005**, *40*, 715.